2006

A Fast Parallelized Computational Approach Based on Sparse LU Factorization for Predictions of Spatial and Time-Dependent Currents and Voltages in Full-Body Biomodels

Ashutosh Mishra
Old Dominion University

Ravindra P. Joshi
Old Dominion University

Karl H. Schoenbach
Old Dominion University

C. D. Clark III

Original Publication Citation

Mishra, A., Joshi, R. P., Schoenbach, K. H., & Clark, C. D. (2006). A fast parallelized computational approach based on sparse LU factorization for predictions of spatial and time-dependent currents and voltages in full-body biomodels. *IEEE Transactions on Plasma Science, 34*(4), 1431-1440. doi:10.1109/tps.2006.876485

A Fast Parallelized Computational Approach Based on Sparse LU Factorization for Predictions of Spatial and Time-Dependent Currents and Voltages in Full-Body Biomodels

Ashutosh Mishra, Ravindra P. Joshi, *Senior Member, IEEE*,
Karl H. Schoenbach, *Fellow, IEEE*, and C. D. Clark, III

Invited Paper

***Abstract*—Realistic and accurate numerical simulations of electrostimulation of tissues and full-body biomodels have been developed and implemented. Typically, whole-body systems are very complex and consist of a multitude of tissues, organs, and subcomponents with diverse properties. From an electrical standpoint, these can be characterized in terms of separate conductivities and permittivities. Accuracy demands good spatial resolution; thus, the overall tissue/animal models need to be discretized into a fine-grained mesh. This can lead to a large number of grid points (especially for a three-dimensional entity) and can place prohibitive requirements of memory storage and execution times on computing machines. Here, the authors include a simple yet fast and efficient numerical implementation. It is based on LU decomposition for execution on a cluster of computers running in parallel with distributed storage of the data in a sparse format. In this paper, the details of electrical tissue representation, the fast algorithm, the relevant biomodels, and specific applications to whole-animal studies of electrostimulation are discussed.**

***Index Terms*—Distributed currents, LU decomposition, parallel computing, tissue modeling, whole body.**

I. Introduction

ELECTRICAL excitation, which has been used to stimulate both the central and the peripheral nervous system, has a variety of potential diagnostic and therapeutic applications [1]–[3]. For example, electrically stimulated neurogenesis is a potential tool for enabling the production of new nerve cells from neuronal stem cells [4], [5]. It is used in implantable devices for neuromuscular stimulation; these devices are designed to control the contraction of paralyzed skeletal muscles, thereby producing functional movements in patients with stroke and spinal cord injuries [6], [7]. Electrical excitation is also a useful tool to study the properties and functions of nerves (including the brain) and muscles (including the heart). It also provides information on strength–duration characteristics, including the inherent time constants. Excitation with ultrashort pulses is also an important issue for the health and safety assessment of ultrawideband (UWB) sources, which produce nanosecond pulses. This issue has been discussed at length elsewhere [8].

In general, muscle excitation can be achieved either remotely through the principle of electromagnetic induction [9]–[11] or directly through electrical contact [12]. UWB pulses have not, to date, shown significant, robust, and reliable biological effects. Such UWB studies using rats probed behavioral teratology, heart rate, blood pressure, brain histology, and genetic alterations [13]–[16]. This contribution focuses on pulsed excitation delivered to biological tissues (and whole bodies) through direct electrical contacts. Thus, it is assumed that electrodes can be directly applied on the muscle/tissue surface, and motor nerve fibers within the muscle are then excited by the potential created within the muscle by the external source. In general, the potential can also be applied through a conductive medium surrounding the biomass as discussed in a previous report [17].

The use of ultrashort electrical pulses in this context is an emerging topic of interest [18]. Such pulses of nanosecond duration have been shown to have the ability to penetrate the outer (plasma) membrane—without affecting it—to create large trans-membrane potentials across subcellular organelles [19]. Thus, for example, triggering of neurotransmitter or calcium release is possible through the use of ultrashort pulses [20]. Use of this new technology to study submicrosecond pulse widths might reveal new biological phenomena.

The current study was driven, in part, from health and safety concerns of electrostimulation. The overall goal is to understand, quantify, and predict possible adverse electrophysiological changes, including electrically induced organ failures in humans and whole animals, due to electrostimulation. As first discussed by McNeal [21], this overall objective requires a two-step approach. The first essential component is the development

Manuscript received January 7, 2006; revised March 31, 2006. This work was supported in part by the National Training and Information Center (NTIC) and in part by the Air Force Office of Scientific Research (AFOSR), U.S. Air Force.

A. Mishra, R. P. Joshi, and K. H. Schoenbach are with the Department of Electrical and Computer Engineering, Old Dominion University, Norfolk, VA 23529-0246 USA (e-mail: rjoshi@odu.edu).

C. D. Clark, III, is with General Dynamics, Radio Frequency Radiation Branch, AFRL/HEDR, Brooks City Base, San Antonio, TX 78235-5417 USA (e-mail: Clifton.Clark.ctr@brooks.af.mil).

Color versions of Figs. 1 and 3–19 are available online at http://ieeexplore.org.

Digital Object Identifier 10.1109/TPS.2006.876485

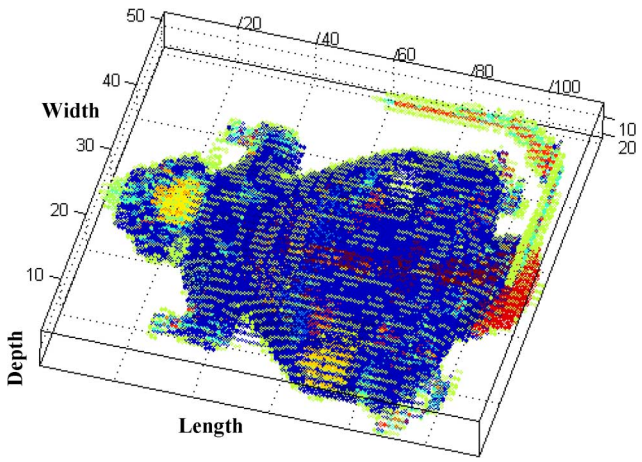

Fig. 1. Rat model enclosed in a simulation box. Dimensions are in millimeters.

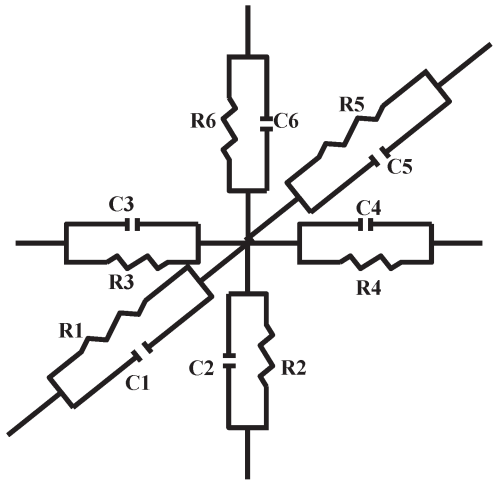

Fig. 2. Schematic of the discretized electrical model used.

of a numerical model for quantifying the microscopic currents and electrically induced potentials due to an external voltage pulse in whole-body systems. Such capability can also provide a useful tool for optimal electrode design and placement. The second step is to use the derived excitation potentials within the whole-body system to determine the biological response of nerves, muscles, and related electrochemical reactions. Here, in this contribution, our focus is on the first part—the development of an efficient numerical model for predicting the voltage-induced currents and potentials.

The whole-body system is very complex and consists of a multitude of tissues, organs, and subcomponents with diverse properties. From an electrical standpoint, these can all be characterized in terms of separate electrical properties, such as conductivity and permittivity. Accuracy demands good spatial resolution, and so the overall whole-animal system needs to be discretized into a fine-grained mesh of individual grid points. The result, especially for a three-dimensional (3-D) entity, is that a very large number of grid points would typically be required for the numerical computations. The requirements for memory storage and execution times on computing machines can quickly become prohibitive in such situations. Here, we include a simple yet fast numerical implementation for execution in parallel on a system of computers (parallelized cluster computing). The details of this fast algorithm and its implementation are given, followed by a specific application to whole-animal studies of electrostimulation.

II. Simulation Method

In the present approach for voltage and current calculations, the entire simulation volume is first discretized into a distributed array of uniformly spaced grid points within a cubic simulation volume. The simulation volume encompasses the entire biomass (i.e., full-animal body) under study. Due to the nonrectangular and curved nature of the full animal objects placed within the simulation box, regions of surrounding air are also included in the cubic region. Thus, irrespective of the actual irregular shape of a body, each raw numerical file involves a regular encompassing volume, as illustrated in Fig. 1. This figure shows a volumetric visualization of the entire rat data present in the corresponding raw model file. Fig. 1 also highlights different tissue types by different colors. The entire simulation box is divided into a Cartesian grid of points (N_x, N_y, and N_z along the three axes). Thus, each grid point has at most a total of six nearest neighbors. For electrical computations, the nearest neighbor sub-regions were represented in terms of a parallel resistor–capacitor combination to account for both conduction and displacement current flows within the biosystem. In essence, a distributed RC model interconnected to (at most) six neighbors was used for the electrical representation. This is shown schematically in Fig. 2. The applied voltage was taken to be a user-specified time-dependent input waveform for the numerical solution, and we essentially imposed Dirichlet boundary conditions locally. Neumann boundary conditions of zero net current flow were applied on all other boundary regions that did not contain any electrodes. For simplicity, the passive RC elements were chosen to be linear, and hence, had fixed values based on the conductivity (σ) and permittivity (ε) characteristics of the local region. Inasmuch as the entire body consists of a large multitude of tissue types, a range of σ and ε values was obtained from actual data[1] and stored in a look-up table. As an example, Table I gives the electrical properties of some tissues that were used in this modeling study.

The application of current continuity at each node then results in a set of coupled equations for the node voltages, which can be solved at each time step. Time-dependent values of the potential across each discretized subregion and current distributions can then be directly obtained. In theory, the voltages can be obtained through Kirchhoff's node analysis. At each node, equations of the type

$$\Sigma\left[(A\varepsilon/L)d\{\Delta V\}/dt + \{\Delta V\}(A\sigma/L)\right] = 0 \qquad (1)$$

apply with A being the elemental cross-sectional area and L the length of each segment. These can be cast into the matrix form

$$[M]\left[\Delta V|_{t+dt} - \Delta V|_t\right] = [B(t)] \qquad (2)$$

[1][Online]. Available: ftp://starview.brooks.af.mil/EMF/dosimetry_models/computer_coded_binary_files/

TABLE I
ELECTRICAL PARAMETERS FOR VARIOUS CONSTITUENT TISSUES

TissueName	Tissue ID	Sigma	Epsilon (real part)
AIR.(external)	0	0	1.00E+00
AIR.(internal)	1	0	1.00E+00
BILE	2	1.4	4.00E+00
BODY.FLUID	3	1.5	4.00E+00
EYE.(cornea)	4	0.4	4.00E+00
FAT	5	0.01	2.50E+00
LYMPH	6	0.5	4.00E+00
MUSCOUS.MEMBRANE	7	0.0004	4.00E+00
NAILS.(toes.and.fingers)	8	0.02	2.50E+00
NERVE.(spine)	11	0.006	4.00E+00
MUSCLE.	17	0.2	4.00E+00
HEART	25	0.05	4.00E+00
WHITE.MATTER	30	0.02	4.00E+00
STOMACH	48	0.5	4.00E+00
GLANDS	49	0.5	4.00E+00
BLOOD.VESSEL	65	0.25	4.00E+00
LIVER	68	0.02	4.00E+00
GALL.BLADDER	88	0.9	4.00E+00
SPLEEN	108	0.03	4.00E+00
CEREBELLUM	110	0.04	4.00E+00
BONE.(cortical)	111	0.02	2.50E+00
CARTILAGE.	133	0.15	4.00E+00
LIGAMENTS	142	0.25	4.00E+00
SKIN/DERMIS	143	0.0002	4.00E+00
INTESTINE.(large)	148	0.01	4.00E+00
TOOTH	152	0.02	2.50E+00
GRAY.MATTER	160	0.02	4.00E+00
EYE.(lens)	163	0.3	4.00E+00
LUNG.(outer)	164	0.2	4.00E+00
INTESTINE.(small)	168	0.5	4.00E+00
EYE.(sclera/wall)	183	0.5	4.00E+00
LUNG.(inner)	184	0.03	2.50E+00
PANCREAS	188	0.5	4.00E+00
BLOOD	189	0.7	4.00E+00
CEREBRALSPINALFLUID	190	2	4.00E+00
EYE.(retina)	203	0.5	4.00E+00
EYE.(aqueous.humour)	204	1.5	4.00E+00
KIDNEYS	207	0.05	4.00E+00
BONE.MARROW	209	0.0005	2.50E+00
BLADDER	227	0.2	2.50E+00
TESTICLES	228	0.4	4.00E+00
PERFECT.CONDUCTOR	229	-1	-1.00E+00
2/3.MUSCLE.	249	0.1333	2.70E+00
PVC	250	0	2.46
FOAM	251	0.0004	1.16
TEM.(old)	252	1.16	1.95
BONE.(cancellous)	253	0.07	2.50E+00
TEM.(new)	254	1.3	5.6
UTAH	255	0.859	39.2

where $[M]$ is a matrix (asymmetric in general), whereas $\Delta V|_t$ and $[B(t)]$ are column vectors. Inasmuch as each node is connected only to six (at most) neighbors, the matrix $[M]$ is extremely sparse. The asymmetry in electrode placement makes $[M]$ nonsymmetric in location and values. Fig. 3 highlights this sparsity by way of a plot of the total elements with respect to the nonzero entries for cubic volumes of varying size. For efficient data storage, one does not really need to set up the matrix in its entirety, but instead only record the small number of nonzero elements.

Mathematically, the desired solution at each time step $\Delta V|_{t+dt}$ can be obtained by inverting $[M]$, and this needs

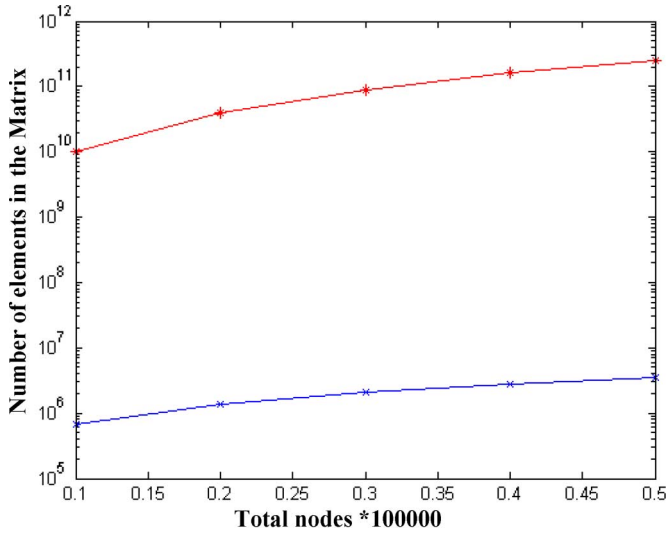

Fig. 3. Sparsity of the resulting coefficient matrix $[M]$. Nonzero values (—×—) (in blue) and total elements (—∗—) (including zeros) for different cases.

to be carried out only once at the beginning. However, from a practical standpoint, if the total number of nodes becomes large (for fine resolution within a whole-body system), then the inversion process becomes prohibitively time consuming and eventually intractable. A practical solution is to make use of the LU decomposition of a matrix. For further speed up and to provide for the large memory storage necessary, the optimal solution is to implement the LU decomposition on a cluster of computers running in parallel with distributed storage of the data in a sparse format. Computational schemes of such nature have recently been devised [22]–[29], and here we discuss our numerical implementation.

The nonsymmetric nature of the matrix $[M]$ eliminates the possibility of using the Cholesky factorization method [30], which is known to be one of the most efficient and fast techniques. The extremely sparse structure of the coefficient matrix $[M]$ led us to adopt SuperLU_DIST. This is a scalable distributed-memory sparse direct solver for asymmetric linear systems [29] for obtaining the node voltages. The details of the algorithm can be found elsewhere [29]. This is a numerically stable approach, and both scalable implementation and scheduling optimization are possible because of the static data structures.

The sparse LU factorization has been shown to be as scalable as the sparse Cholesky factorization method. The current release of the SuperLU_DIST scheme uses Gaussian elimination with static pivoting, and the algorithm is parallelized using message passing interface (MPI). Other features include a two-dimensional (2-D) irregular block-cyclic mapping using a supernodal structure, and a loosely synchronous scheduling with pipelining.

Sparse solvers also deserve mention in this present context because dense storage of the coefficient matrix rapidly makes the solution intractable with increasing node number. For example, a tissue requiring $100 \times 100 \times 10$ nodes would use up $\sim$ 74 GB of memory for an 8-B floating precision. With the

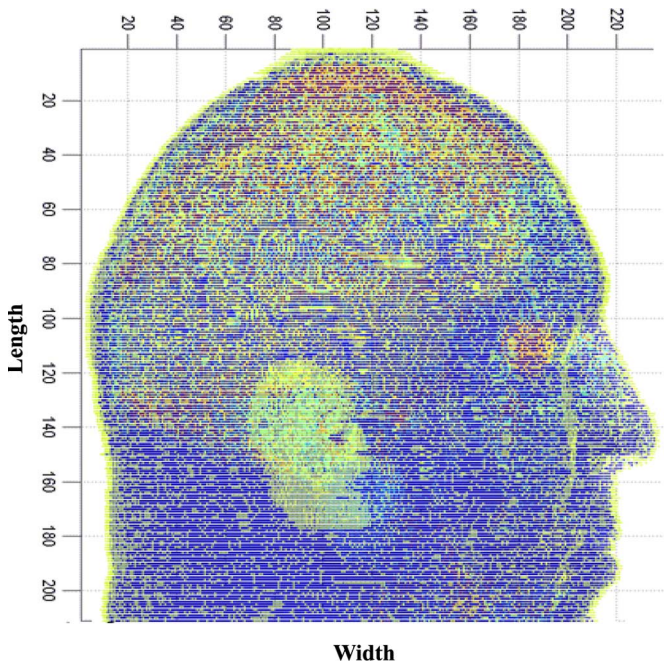

Fig. 4. Human head model from Brooks database with dimensions in millimeters.

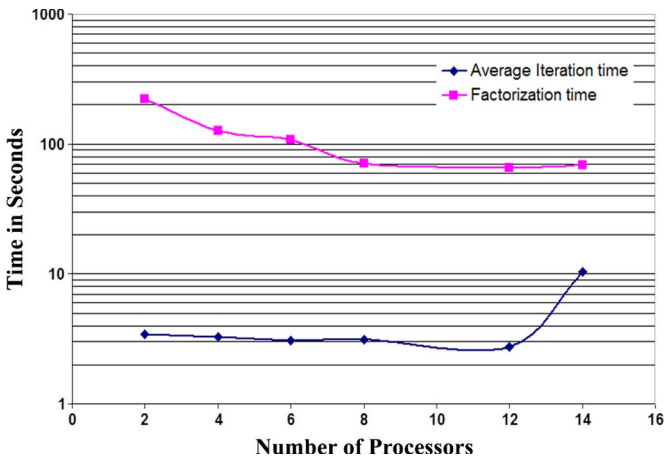

Fig. 5. Dependence of runtime for the 144 000-node rat model as a function of parallel processors.

present sparse setup, the actual number of nonzero entries is 676 000, and this leads to less than 6 MB.

The different biomodels currently characterized at Brooks Base include rat, frog, monkey, and a human head. For computational simplicity, we have chosen to focus on the rat. These models are based on anatomical slices from MRI scans. The rat model consists of 35 types of tissue, whereas the human head (shown in Fig. 4) has 26 tissue types. The spatial resolutions for the rat and human head models were 1 and 3 mm, respectively.

The advantage of utilizing parallel processing capability in the present context is brought out through the "timing diagram" in Fig. 5. The figure shows the factorization time for the $[M]$ matrix for the 144 000-node rat model as a function of the processors used for the computations. Also shown is the average time taken for each iterative step for a pulsed voltage response calculation. Two points are immediately obvious.

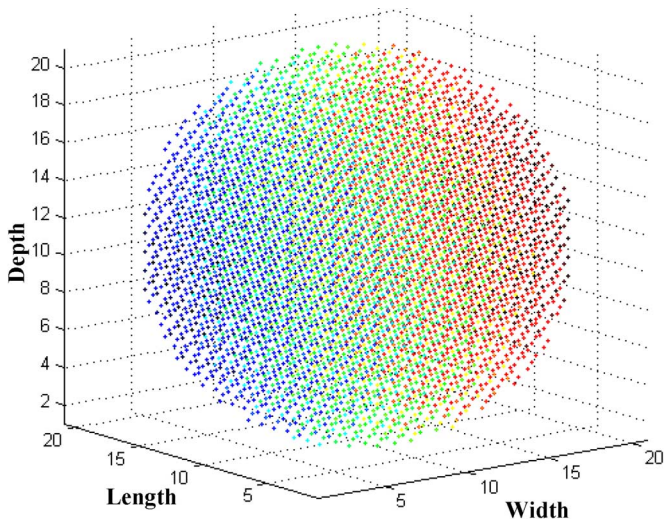

Fig. 6. Plot of spherical tissue embedded in a cube as a simple example.

First, the initial factorization process is very time consuming and represents a large overhead on the overall calculations. Any speed-up in this initial phase is therefore very helpful. Employing several processors greatly reduces this factorization time. A monotonic and logarithmic decrease is predicted as the number of processors increases from 4 to 24. Second, the average duration for each iterative step of the time-dependent calculations decreases dramatically as the number of processors is increased from 4 to 12. Beyond that, the average time for each iteration actually increases somewhat and reaches a saturating limit. This behavior arises from a tradeoff between enhanced average speed and longer time spent in communications between the various processors as their numbers are increased. Clearly, for simulations involving short voltage pulses (e.g., the nanosecond pulsars [17]), it would be very advantageous to use a large number of parallel processors as the factorization overhead would then be a significant percentage.

III. Results and Discussions

A. Test Case of Uniform Hemisphere in Saline

A test case was first analyzed to gauge the validity of the numerical implementation of the simulation tool. A simple data file containing a single tissue type (muscle) was chosen. The geometry was a spherical mass surrounded by air in a cube. The corresponding 3-D plot is shown in Fig. 6. A slice across the bottommost surface (identical to that at the other five faces of the cube) extracted from the data file is shown in Fig. 7. The centrally located circular region is the tissue. In the present case, electrodes were applied to the top and bottom slices for the purposes of obtaining the time-dependent current response.

The simulated current is shown in Fig. 8 for a trapezoidal pulse with 30-ns rise and fall times, and 500-ns on time. The tissue conductivity (σ) used was 1.33×10^{-3} $(\Omega \cdot \mathrm{cm})^{-1}$, whereas the dielectric constant was 2.7. A steady-state current of ~ 8 A is predicted during the pulse on time. The voltage profile across a cross-sectional slice passing through the spherical center and the two electrodes is given in Fig. 9.

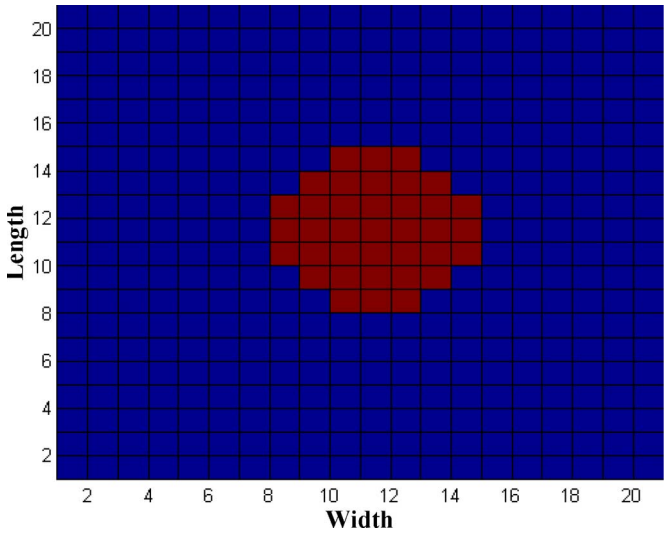

Fig. 7. Plot of the tissue end-slice for the data in Fig. 6.

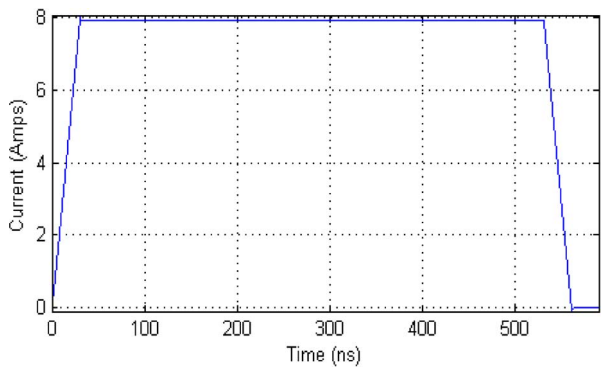

Fig. 8. Simulated current response to trapezoidal pulse.

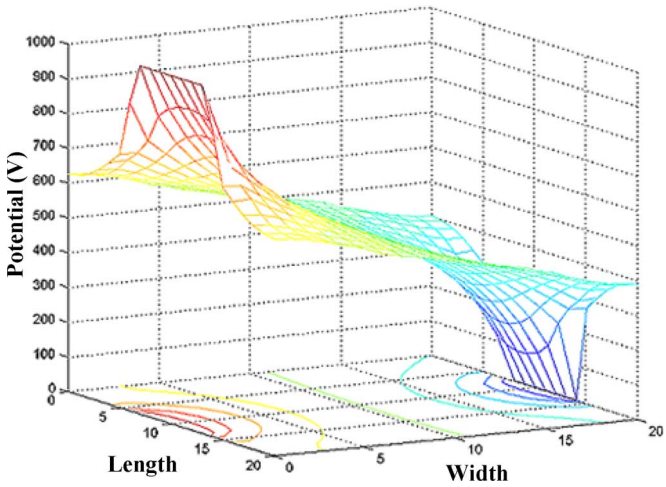

Fig. 9. Potential profile in a plane through the electrodes and sphere center.

Next, a slightly different electrode placement for the simple tissue in saline was carried out as a validity check. The cathode was assumed to be a planar disk passing through the center of the spherical tissue, with the anode being a smaller circular disk cutting the sphere parallel to the cathode. Thus, a 2-D projection of the geometry, as shown in Fig. 10, resulted. In Fig. 10, the cathode is represented by the diameter on the left, whereas the

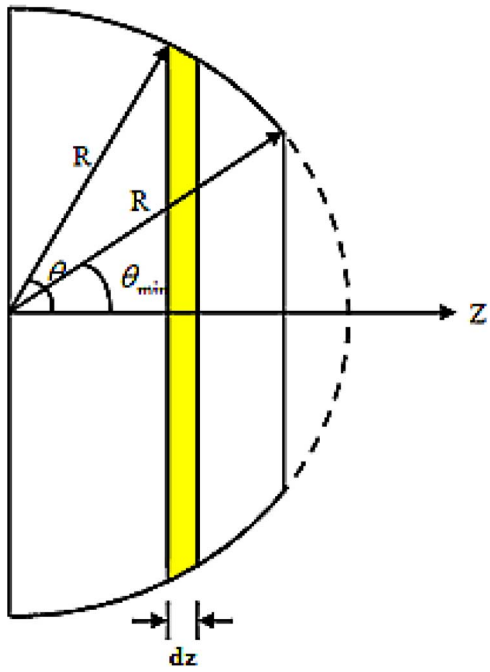

Fig. 10. 2-D projection for the geometry used in the simulation.

circular anode plate is the solid line on the right. The anode is parallel to the cathode and cuts the sphere in a circular disk. In spherical coordinates, the maximum angle between the peripheral anode point and the spherical center is $\theta_{\min}$. The radius of the sphere is denoted by R, the perpendicular distance between the two parallel electrodes is along the z-axis, and θ is a general angle with $\theta_{\min} < \theta < \pi/2$. The effective resistance R_{eff} of the tissue between the two electrodes can be computed analytically.

Considering a differential slice of thickness dz as shown in Fig. 10, the corresponding differential resistance dR_{eff} is

$$dR_{\text{eff}} = dz/[\sigma \text{ Area}] \tag{3a}$$

where the area of the differential disk $= \pi[R\sin(\theta)]^2$. Also, $z = R\cos(\theta)$, from which $dz = -R\sin(\theta)d\theta$, and the total effective resistance R_{eff} becomes

$$R_{\text{eff}} = \int_{-\pi/2}^{\theta\,\min} \left\{ R\sin(\theta)d\theta \Big/ \left[\sigma\pi \left\{R\sin(\theta)\right\}^2\right]\right\}. \tag{3b}$$

Carrying out the integration yields the effective resistance for the geometry

$$R_{\text{eff}} = -\left\{\ln\left[\tan(\theta_{\min}/2)\right]\right\}/\{\sigma\pi R\}. \tag{3c}$$

The simulation result for the current response to a 1000-V trapezoidal pulse (0.5-ns rise and fall times and 10-ns on time) is shown in Fig. 11. The predicted stabilized current during the pulse on time was roughly 51.5 A.

The effective resistance from the numerical simulation works out to be $1000\ \text{V}/51.5\ \text{A} = 19.42\ \Omega$. The analytical formula in (3c) yields for the $1.33 \times 10^{-3}\ (\Omega \cdot \text{cm})^{-1}$ conductivity

$$R_{\text{eff}} = -\left\{\ln\left[\tan(\theta_{\min}/2)\right]\right\}/\{1.333 \times 10^{-3}\,\pi 10\}\ \Omega. \tag{4}$$

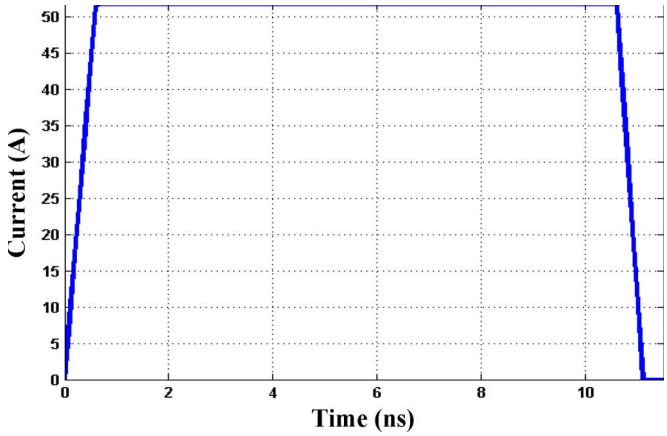

Fig. 11. Current response to a trapezoidal applied pulse.

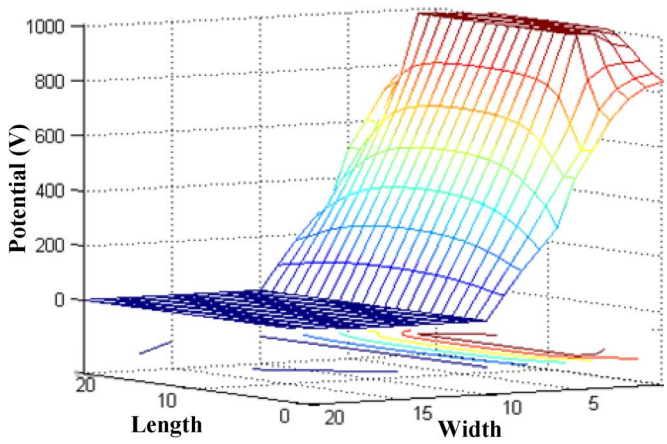

Fig. 12. Potential profile at 5.775 ns for the spherical tissue.

The angle θ here is given by $\theta = \cos^{-1}\{7/10\} = 0.7954$ rd. Using this value in (4) yields $R_{\text{eff}} \sim 20.7\ \Omega$. This value is very close to the simulation result of 19.42 Ω and roughly validates the numerical implementation in this case.

The voltage profiles for the above test simulation are presented in Fig. 12 below. The maximum voltage at the anode is 1000 V and occurs over a flat region intersecting the sphere. The cathode is at 0 V and runs through the parallel diameter. Most of the voltage drop occurs between the two electrodes. Some electric field is also created near the smaller anode disk.

B. Simulations for the Rat Model

Next, simulations for the rat model are discussed. Fig. 13 shows the bottom view of a discretized picture of the rat used. The axes scale are in millimeters, and the length of the box containing the rat model is about 120 mm, whereas the breadth and depth are roughly 60 and 20 mm, respectively. For the 1-mm spatial resolution, this translates into a total of 144 000 nodes. The whole mouse model contained various internal organs and body parts. Whereas the details are quite complicated and difficult to visualize in very aspect, a rough perception can be offered by taking various slices perpendicular to the depth.

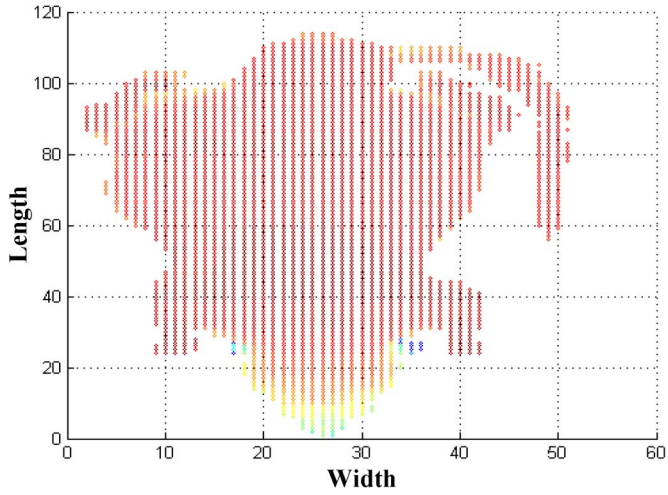

Fig. 13. Bottom view of a model rat mouse used for numerical calculations.

The contour plots in Fig. 14 show cross-sectional slices at depths of 5, 10, and 18 mm from the top. Corresponding contours of the permittivity across the cross sections are given in Fig. 15.

The results of the internal potential generated within the rat in response to an external voltage pulse are shown and discussed next. For simplicity, a trapezoidal pulse of nanosecond duration, with rise and fall times of 1 ns and an on time of 10 ns, was assumed. This shape and duration are in keeping with the actual experimental pulses being used by several research groups [31]. The voltage profile at the midpoint of about 5.775 ns is given in Fig. 16. The lowest slice with the four feet and tail was grounded. A uniform potential of 1000 V was assumed at the topmost plane parallel to the ground. As before, cross-sectional slices were chosen perpendicular to the depth axis for visualization. A "top view" showing the tissue layout across the chosen slice is given in Fig. 16, whereas Fig. 17 shows the 3-D potential profile corresponding to the tissue. The four "grounded" legs are evident.

A more realistic pulse with a waveshape typically generated by the pulsars at Brooks City Base was used as a final test of the numerical model. Results for the applied voltage pulse and current are shown in Fig. 18. The current is seen to track the external voltage fairly accurately. The displacement currents are relatively minor. Here, a comment pertaining to muscular twitching or similar electrostimulation by such pulses is perhaps necessary and relevant. The nerve or muscular response is directly related to the amount of charge deposited into the biosystem [32], [33]. Hence, for maximal effect with high efficiency, a monopolar voltage pulse with a fast rise time would appear to be the optimal choice. The Brooks pulse shown in Fig. 18 is fairly oscillatory and perhaps not the most efficient for electrostimulation.

The time-dependent voltage evolution inside the model rat across a line parallel to the ground is shown in Fig. 19. The line was located at a depth of 10 mm, midway along the longitudinal axis, and was chosen to run across the entire 51-mm width. The oscillatory potential at any point on the chosen line is evident. Although not shown, the potential difference across any chosen segment or set of points could be obtained at every time step.

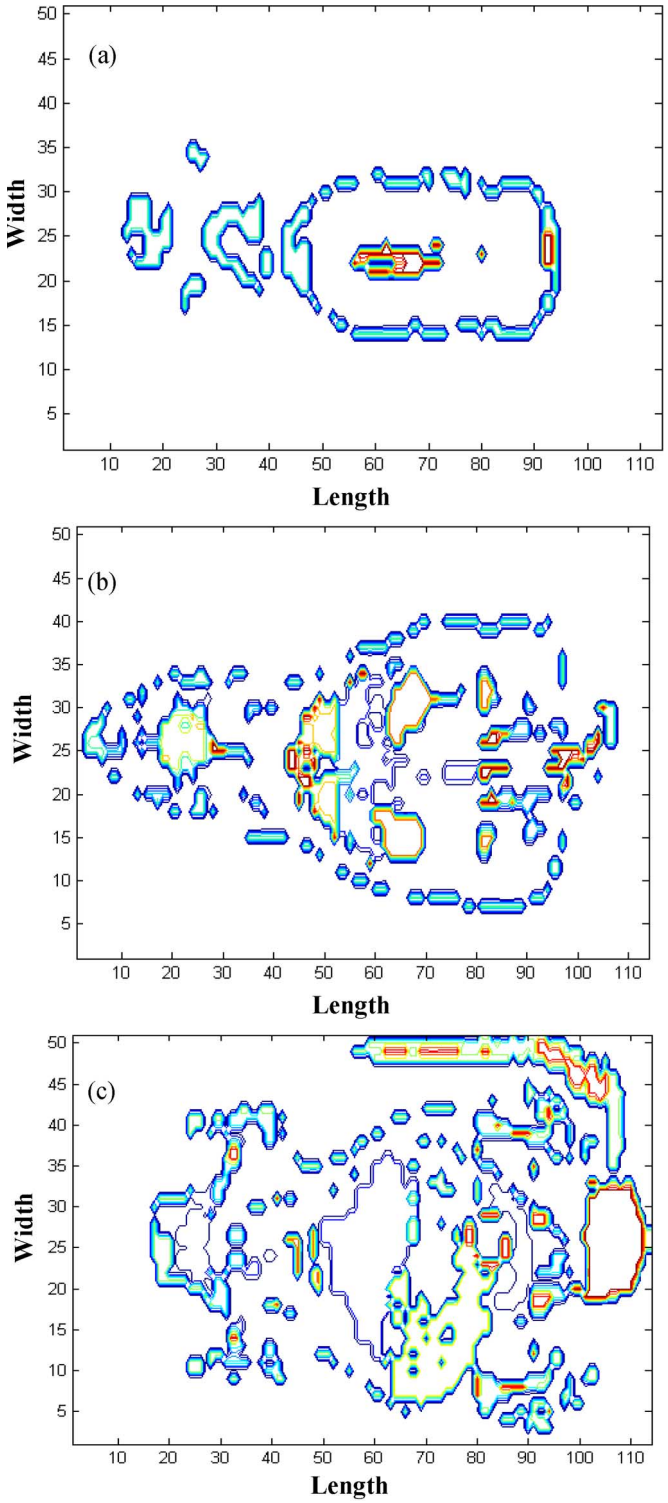

Fig. 14. Cross sections of the mouse at different depths starting from the top. (a) 5 mm, (b) 10 mm, and (c) 18 mm along the depth.

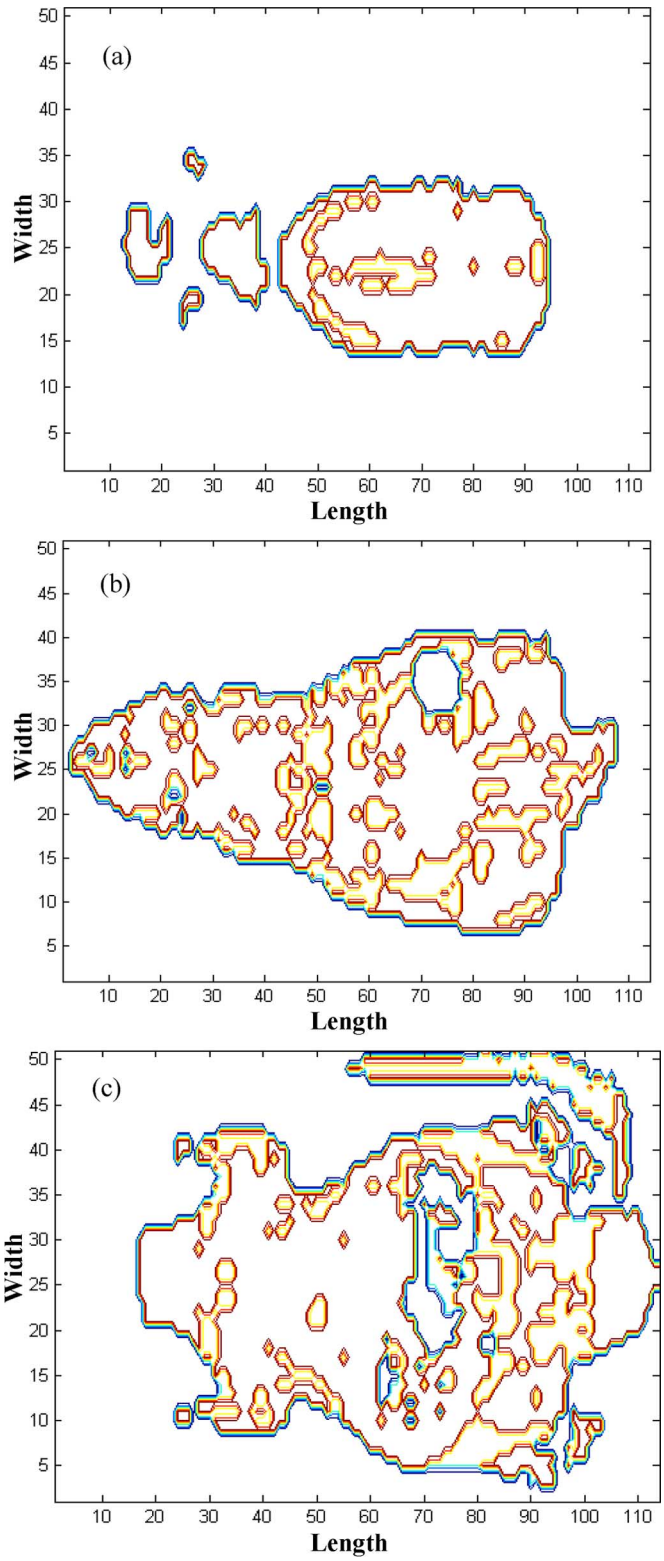

Fig. 15. Cross-sectional contours of the tissue permittivities for the rat model.

The data also allowed for the evaluation of other parameters of interest, such as the "activating function" for twitching [34], at any point inside the rat.

IV. Conclusion

Electrostimulation has been used for a variety of diagnostic and therapeutic applications. Excitation with electrical pulses is also an important issue in the context of health and safety assessment of various UWB sources. An important first step in accurately predicting the bioresponse to such an electrical stimulation is the development of numerical models for quantifying the currents and potentials induced electrically within whole-body systems. A side benefit of such a

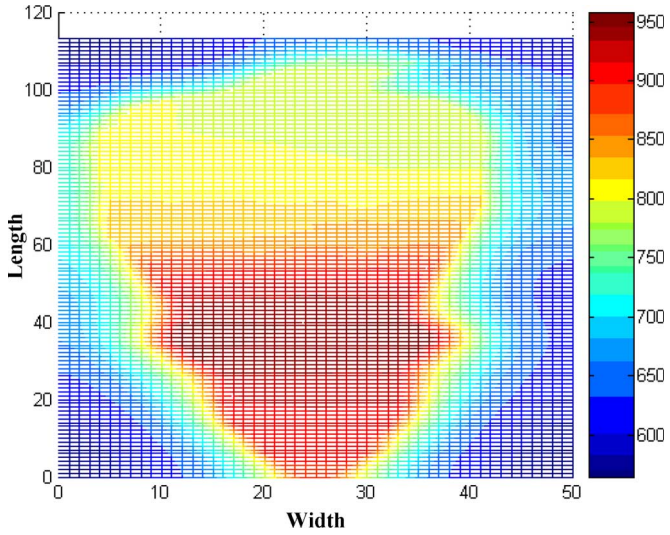

Fig. 16. 5.775-ns top view of the potential profile at a depth of 12 mm.

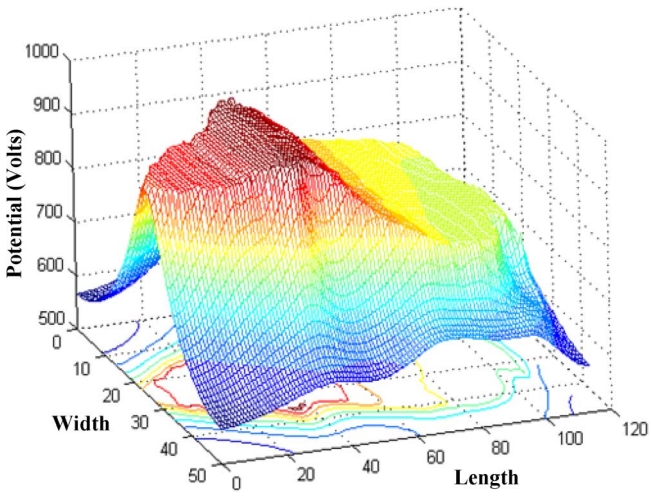

Fig. 17. 5.775-ns perspective of the potential profile at a depth of 12 mm.

simulation is the capability for optimal electrode design and placement.

Typically, whole-body systems are very complex and consist of a multitude of tissues, organs, and subcomponents with diverse properties. From an electrical standpoint, these can be characterized in terms of separate conductivities and permittivities. Accuracy demands discretization of the entire simulation volume into a fine-grained mesh. Practically, this can place prohibitive computational requirements on memory storage and execution times. This makes numerical simulations an arduous task. Here, we have presented a simple yet fast and efficient numerical implementation for easing the computational difficulty. A distributed LU decomposition in sparse format was employed for execution on a cluster of computers running in parallel. We successfully implemented our numerical model and successfully tested on a 1-mm spatially resolved rat model. It was quantitatively shown that increasing the processors reduces the computational time. Both simple trapezoidal pulses and more realistic waveshapes from actual pulsars were used. Future work would include the development of a multilevel multigrid capability for finer detail.

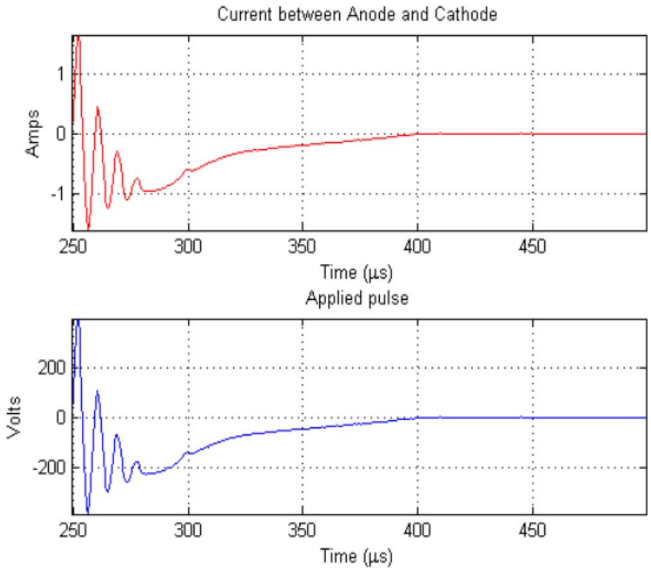

Fig. 18. Simulated current response to a voltage pulse for the rate biomodel with the same waveshape as typically used at Brooks City Base.

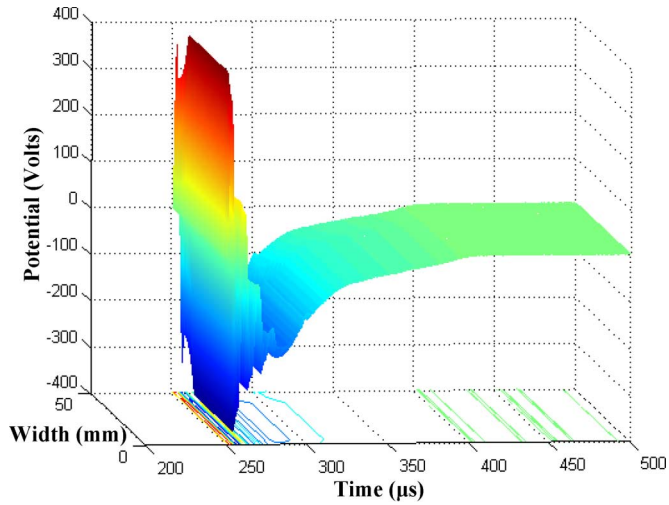

Fig. 19. Simulated potential evolution across a line running along the entire 51-mm width of the rat model. The line was located at a depth of 10 mm, at the midpoint of the longitudinal axis.

ACKNOWLEDGMENT

The authors would like to thank S. Li (Lawrence Berkeley National Laboratory), A. Tarafdar (ODU), and J. Kolb (ODU) for useful discussions. The opinions expressed herein are solely those of the authors.

REFERENCES

[1] P. J. Basser and B. J. Roth, "New currents in electrical stimulation of excitable tissue," *Annu. Rev. Biomed. Eng.*, vol. 2, pp. 377–397, Aug. 2000.
[2] J. P. Reilly, *Electrical Stimulation and Electropathology*. Cambridge, U.K.: Cambridge Univ. Press, 1992.
[3] B. J. Roth, "Mechanisms for electrical stimulation of excitable tissue," *Crit. Rev. Biomed. Eng.*, vol. 22, no. 3/4, pp. 253–305, 1994.
[4] P. S. Eriksson, E. Perfilieva, T. Bjork-Eriksson, A. M. Alborn, C. Nordborg, D. A. Peterson, and F. H. Gage, "Neurogenesis in the adult human hippo-campus," *Nat. Med.*, vol. 4, no. 11, pp. 1313–1317, Nov. 1998.

[5] E. Gould, A. J. Reeves, M. S. Graziano, and C. G. Gross, "Neurogenesis in the neocortex of adult primates," *Science*, vol. 286, no. 5439, pp. 548–552, Oct. 1999.
[6] F. Rattay, *Electrical Nerve Stimulation: Theory, Experiments and Applications*. New York: Springer-Verlag, 1990.
[7] D. M. Durand, "Electrical stimulation of excitable tissue," in *The Biomedical Engineering Handbook*, J. D. Bronzino, Ed. Boca Raton, FL: CRC Press, 1995, pp. 229–251.
[8] W. R. Rogers, J. H. Merritt, J. C. Comeaux, Jr., C. T. Kuhnel, D. F. Moreland, D. G. Teltschik, J. H. Lucas, and M. R. Murphy, "Strength–duration curve for an electrically excitable tissue extended down to near 1 nanosecond," *IEEE Trans Plasma Sci.*, vol. 32, no. 4, pp. 1587–1599, Aug. 2003.
[9] K. P. Esselle and M. A. Stuchly, "Neural stimulation with magnetic fields: Analysis of induced electric fields," *IEEE Trans. Biomed. Eng.*, vol. 39, no. 7, pp. 693–700, Jul. 1992.
[10] L. Heller and D. B. van Hulsteyn, "Brain stimulation using electromagnetic sources: Theoretical aspects," *Biophys. J.*, vol. 63, no. 1, pp. 129–138, Jul. 1992.
[11] P. J. Basser and B. J. Roth, "Stimulation of a myelinated nerve axon by electromagnetic induction," *Med. Biol. Eng. Comput.*, vol. 29, no. 3, pp. 261–282, May 1991.
[12] J. H. Meier, W. L. C. Rutten, A. E. Zoutman, H. B. K. Boom, and P. Bergveld, "Stimulation of multipolar fiber selective neural stimulation using intrafascicular electrodes," *IEEE Trans. Biomed. Eng.*, vol. 39, no. 2, pp. 122–134, Feb. 1992.
[13] B. L. Cobb, J. R. Jauchem, P. A. Mason, M. P. Dooley, S. A. Miller, J. M. Ziriax, and M. R. Murphy, "Neural and behavioral teratological evaluation of rats exposed to ultra-wideband electromagnetic fields," *Bioelectromagnetics*, vol. 21, no. 7, pp. 524–537, Oct. 2000.
[14] J. R. Jauchem, M. R. Frei, K. L. Ryan, J. H. Merritt, and M. R. Murphy, "Lack of effects on heart rate and blood pressure in ketamine-anesthetized rats briefly exposed to ultra-wideband electromagnetic pulses," *IEEE Trans. Biomed. Eng.*, vol. 46, no. 1, pp. 117–120, Jan. 1999.
[15] R. L. Seaman, M. R. Vijayalaxmi, M. L. Belt, J. M. Doyle, S. P. Mathur, and T. J. Prihoda, "Frequency of micronuclei in the blood and bone marrow cells of mice exposed to ultra-wideband electromagnetic radiation," *Int. J. Radiat. Biol.*, vol. 75, no. 1, pp. 115–120, Jan. 1999.
[16] S. A. Miller, M. E. Bronson, and M. R. Murphy, "Ultrawideband radiation and pentylenetetrazol-induced convulsions in rats," *Bioelectromagnetics*, vol. 20, no. 5, pp. 327–329, 1999.
[17] R. P. Joshi, F. Chen, and W. R. Rogers, "Modeling electrode-based stimulation of muscle and nerve by ultra-short electric pulses," *IEEE Trans. Plasma Sci.*, vol. 32, no. 4, pp. 1687–1695, Aug. 2004.
[18] R. P. Joshi, Q. Hu, R. Aly, K. H. Schoenbach, and H. P. Hjalmarson, "Self-consistent simulations of electroporation dynamics in biological cells subjected to ultrafast electrical pulses," *Phys. Rev. E, Stat. Phys. Plasmas Fluids Relat. Interdiscip. Top.*, vol. 64, no. 1, pp. 11913/01–11913/13, 2001.
[19] R. P. Joshi, Q. Hu, and K. H. Schoenbach, "Modeling studies of cell response to ultrashort, high-intensity electric fields—Implications for intracellular manipulation," *IEEE Trans. Plasma Sci.*, vol. 32, no. 4, pp. 1677–1686, Aug. 2004.
[20] T. P. Vernier, Y. Sun, L. Marcu, S. Salemi, C. M. Craft, and M. A. Gundersen, "Calcium bursts induced by nanosecond electric pulses," *Biochem. Biophys. Res. Commun.*, vol. 310, no. 2, pp. 286–295, Oct. 2003.
[21] D. R. McNeal, "Analysis of a model for excitation of myelinated nerve," *IEEE Trans. Biomed. Eng.*, vol. BME-23, no. 4, pp. 329–337, Jul. 1976.
[22] T. Imamura, "An estimation of complexity and computational costs for vertical block-cyclic distributed parallel LU factorization," *J. Supercomput.*, vol. 15, no. 1, pp. 95–110, Jan. 2000.
[23] D. Kaya and K. Wright, "Parallel algorithms for LU decomposition on a shared memory multiprocessor," *Appl. Math. Comput.*, vol. 163, no. 1, pp. 179–192, Apr. 2005.
[24] J. M. Conroy, S. G. Kratzer, R. F. Lucas, and A. E. Naiman, "Parallel sparse LU factorization," *SIAM J. Sci. Comput.*, vol. 19, no. 2, pp. 584–604, 1998.
[25] K. Shen, T. Yang, and X. Jiao, "Efficient 2D sparse LU factorization on parallel machines," *SIAM J. Matrix Anal. Appl.*, vol. 22, no. 1, pp. 282–305, 2001.
[26] M. Hahad, "A parallel sparse LU decomposition with application to semiconductor device simulation," *Lect. Notes Comput. Sci.*, vol. 1300, pp. 848–851, Sep. 1997.
[27] P. Chen, H. Runesha, D. T. Nguyen, P. Tong, and T. Y. P. Chang, "Sparse algorithms for indefinite system of linear equations," *Comput. Mech.*, vol. 25, no. 1, pp. 33–42, 2000.
[28] J. A. George and W. H. Liu, *Computer Solution of Large Sparse Positive Definite Systems*. Englewood Cliffs, NJ: Prentice-Hall, 1981.
[29] X. S. Li and J. W. Demmel, "SuperLU-DIST: A scalable distributed-memory sparse direct solver for unsymmetric linear systems," *ACM Trans. Math. Softw.*, vol. 29, no. 2, pp. 110–140, Jun. 2003.
[30] A. George, J. W. H. Liu, and E. Ng, "Communication results for parallel sparse Cholesky factorization on a hypercube," *Parallel Comput.*, vol. 10, no. 3, pp. 287–298, May 1989.
[31] A. G. Pakhomov, A. Phinney, J. Ashmore, K. Walker, III, J. F. Kolb, S. Kono, K. H. Schoenbach, and M. R. Murphy, "Characterization of the cytotoxic effect of high-intensity, 10-ns duration electrical pulses," *IEEE Trans. Plasma Sci.*, vol. 32, no. 4, pp. 1579–1586, Aug. 2004.
[32] H. A. Blair, "On the intensity–time relations for stimulation by electric currents, I," *J. Gen. Physiol.*, vol. 15, no. 6, pp. 709–721, Jul. 1932.
[33] ——, "On the intensity–time relations for stimulation by electric currents, II.," *J. Gen. Physiol.*, vol. 15, no. 6, pp. 731–755, Jul. 1932.
[34] F. Rattay, "Analysis of models for external stimulation of axons," *IEEE Trans. Biomed. Eng.*, vol. BME-33, no. 10, pp. 974–977, Oct. 1986.

Ashutosh Mishra received the B.E. degree from Manipal Institute of Technology, Karnataka, India, in 1999, and the M.S. degree from Old Dominion University, Norfolk, VA, in 2003, both in electrical engineering. He is currently working toward the Ph.D. degree in the Department of Electrical and Computer Engineering, Old Dominion University.

He was a Senior Engineer (R&D) with LML-Vespa between July 1999 and May 2001. His research interests include computational methods, high-performance computing, and signal processing.

Ravindra P. Joshi (M'83–SM'95) received the B.Tech. and M.Tech. degrees from the Indian Institute of Technology, Bombay, India, in 1983 and 1985, respectively, and the Ph.D. degree from Arizona State University, Tempe, in 1988, all in electrical engineering.

He was a Post-Doctoral Fellow with the Center of Solid State Electronics Research, Arizona State University. He was a Visiting Scientist with Oak Ridge National Laboratory, Philips Laboratory, Motorola, and NASA Goddard in the past. In 1989, he joined the Department of Electrical and Computer Engineering, Old Dominion University, Norfolk, VA, as an Assistant Professor. He is currently a Full Professor and involved in research for broadly encompassing modeling and simulations of charge transport, nonequilibrium phenomena, and bioelectrics. He has also used Monte Carlo methods for simulations of high-field transport in bulk and quantum well semiconductors. He has authored over 70 journal publications.

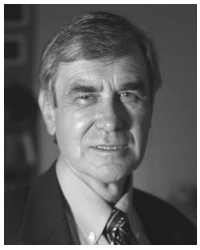

Karl H. Schoenbach (SM'82–F'94) received the Diploma and Dr.rer.nat. degrees in physics from the Technische Hochschule Darmstadt (THD), Darmstadt, Germany, in 1966 and 1970, respectively.

From 1970 to 1978, he was with the THD where he worked in the areas of high pressure gas discharge physics and on the dense plasma focus. From 1979 to 1985, he held a faculty position with Texas Tech University, where he was involved in research on fast-opening switches, especially electron beam and laser-controlled diffuse discharge opening switches. In 1985, he joined Old Dominion University, in Norfolk, VA. He was active in research on photoconductive switches until 1993, and has now concentrated his research efforts on high-pressure glow discharges, glow (streamer) discharges in liquids, and on environmental and medical applications of pulse power technology.

Mr. Schoenbach has chaired a number of workshops and conferences, among them the 1991 IEEE International Conference on Plasma Science and the First International Symposium on "Nonthermal Medial/Biological Treatments Using Electromagnetic Fields and Ionized Gases" or "ElectroMed99." He received the High Voltage Award at the 2000 High Voltage Workshop, sponsored by the IEEE Dielectrics and Electrical Insulation Society. He was the Guest Editor of the IEEE TRANSACTIONS ON ELECTRON DEVICES (1990) and the IEEE TRANSACTIONS ON PLASMA SCIENCE (1999), and is presently an Associate Editor of the IEEE TRANSACTIONS ON PLASMA SCIENCE.

C. D. Clark, III received the B.S. degree in physics from Fort Hays State University, Hays, KS, in 2004.

He is currently a Research Physicist with General Dynamics AIS, AFRL/HEDR, Brooks City Base, San Antonio, TX.